

Ultrasonic phosphate bonding of nanoparticles.

By *David C Bassett[§], Geraldine Merle, Bruce Lennox, Reza Rabiei, François Barthelat, Liam M Grover and Jake E Barralet**

[*] Corresponding author Prof. J. E. Barralet, Dr. D. C. Bassett, Dr. G. Merle

Faculty of Dentistry, McGill University, Montreal, H3A 2B2, (Canada)

E-mail: (jake.barralet@mcgill.ca)

Prof. B. Lennox

Department of Chemistry, Faculty of Science, McGill University, Montreal, H3A 2K6,
(Canada)

Dr. R. Rabiei, Prof. F. Barthelat

Department of Mechanical Engineering, Faculty of Engineering, McGill University, Montreal,
H3A 0C3, (Canada)

Dr. L. M. Grover

School of Chemical Engineering, University of Birmingham, Birmingham, B15 2TT, (Great
Britain).

[§] Present address Dr. D. C. Bassett

Department of Physics, Norwegian University of Science and Technology, Trondheim, 7491,
(Norway)

Prof. J. E. Barralet

Department of Surgery, Faculty of Medicine, McGill University, Montreal, (Canada)

Keywords: nanoparticles, ultrasound, catalysis, joining, xerogel

New methods to assemble nanoparticulate materials are required to exploit the third dimension, creating functionality whilst also minimising contamination of the environment and end users. Most nano-assembly techniques either yield fragile materials formed through electrostatic or Van der Waals interactions or are adapted from macro and microscale joining techniques requiring heat to cause melting or solid state diffusion, which in turn can alter nanostructure. Here we report our discovery that low intensity ultrasound-induced radicals interact with surface adsorbed orthophosphate to bond nanoparticles with high mechanical strength.

Collapse of sonically generated cavitation bubbles can damage materials by causing pitting.^[1]

This process and the associated generation of radicals are employed in chemical and particulate syntheses to accelerate reactions and alter the shape, size and phase of the product

and efficiency of reactions.^[2] Here we report the unexpected finding that exposure of orthophosphate-coated nanoparticulate xerogels to low power ($0.2 - 1.4 \text{ W cm}^{-2}$) ultrasound led to irreversible agglomeration to form durable mesoporous assemblies.

Because of the colloidal nature of nanoparticles, avoiding human exposure following contamination of the workplace and environment is challenging^[3] and granulation potentially offers a safer way to handle nanoparticles, but only if the granulates are both durable and functional. Currently the most employed method to assemble nanoparticles into mesoporous materials is by gelation of colloids through *in situ* synthesis or liquid removal, followed by drying at ambient or supercritical pressure to make xero- and aerogels respectively.^[4] Capillary stresses generated upon aqueous meniscus formation in nanopores are typically 100–200 MPa,^[5] however these gels are mechanically weak having tensile strengths of typically only $\sim 150 - 300 \text{ kPa}$ ^[6] and so are destroyed by even trace amounts of liquid which has severely limited the environments in which these gels can function. Prior improvements include combining with a tougher polymer, which is not ideal since this occludes nanoporosity, or sintering which increases particle size and hence reduces the available surface area^[7] and may not be applied to thermally unstable or hydrated materials.

Ultrasound combined with an organic templating agent has previously been reported to synthesise $\sim 200 \text{ nm}$ mesoporous titania particles via a calcination step by fusion of the constituent nanoparticles but was accompanied by a large reduction in surface area.^[8] Ultrasonic welding of solid metallic and plastic components is well known and relies on either self-mating of metals following fragmentation of surface oxides or friction induced melting of plastics. High power ($\sim 40-50 \text{ W cm}^{-2}$) ultrasound has been reported to fuse metallic (Au, Ag, Zn, Ni, Mo, Cr, Sn and Fe) nanoparticles^[9] by local heating from inter-particle collisions, presumably assisted by nanosize related melting point suppression reported to be in the order

of up to 900 °C.^[10] Reports of ultrasonic mediated assembly of ceramics are scarce, however fusion between 200 nm glassy silica particles in water induced by high power (100 W cm⁻²) ultrasound has been reported.^[11] These weak agglomerates appeared transiently and re-fragmented upon continued irradiation. Studies of silica nanoparticle size identified a critical threshold of 200 nm below which fusion did not occur. It was proposed that this was because smaller particles lacked sufficient kinetic energy for silicate bonding between particles.^[12]

We have discovered that when a wide variety of nanopowders dispersed into slurries in a sodium phosphate solution and then air dried to form phosphate-treated xerogels (PTX) were exposed to low power ultrasound, they formed microscale (~200 μm) aggregates that we term phosphate bonded mesoporous microparticles (PBM). This was in stark contrast to phosphate free control (PFC) xerogels that simply fragmented within a few minutes. A wide variety of materials and dissimilar material combinations could be assembled using this technique without sacrificing functional properties. By way of illustration of the wide applicability of the method, we built 1 mm thick porous functional electrodes of the water splitting catalyst cobalt phosphate (CoPi),^[13-15] which is both hydrated and amorphous, and composited this material with 0.3 wt% carbon nanotubes (CNT). This 3D electrode greatly exceeded the inherent efficiency limit of 2D CoPi electrodeposited films caused by electrical conductivity and mass transport which are significant at film thicknesses above ~1 μm.^[14, 16]

Following 5 min ultrasound exposure, both PFC and PTX TiO₂ gel particles had become rounded (cf. **Figure 1a&d**), and showed evidence of surface pitting. After 15 min the PFC had mostly disintegrated into a colloidal suspension that dried as a gel on the sample stub, (Figure 1b) yet PTX comprised two morphologies of microparticles 50-100 μm in dimension; one was smooth and apparently homogeneous (Figure 1e, white arrow), the other consisted of agglomerates of 3-10 μm gel particles (Figure 1e, black arrow). It appeared that these

hierarchically arranged microparticles, themselves consisting of rounded agglomerates of 3–10 μm gel particles (Figure 1e, g-i), were an intermediate stage in the formation of PBM. Closer examination revealed that they were homogeneous at the nanoscale, however the original smaller microparticles from which they were comprised could still be distinguished (Figure 1h). Intriguingly, although these intermediates were clearly formed by particle-particle collision they appeared to have fused plastically since there was no evidence of any angular or flat surfaces normally associated with brittle fracture (Figure 1i). High magnification of the nanoparticulate gel between these smaller subunits did not indicate any gross change in density or primary particle size. This assembly could be due to either a process analogous to plastic deformation previously observed in ceramic particle impaction events^[17] or following isostatic compression of silica aerogels,^[18] or a thermally induced reversible gelation as has been treated theoretically^[19] and observed in an inorganic pyrophosphate gel system.^[20] After 60 min the PFC had completely disintegrated (Figure 1c), whereas PTX derived microparticles treated for 60 min had grown in size to \sim 200 μm and appeared similar to one another (Figure 1f).

Several materials and their combinations could be assembled into PBM such as silver and silver-nanocarbon composites, nickel oxide, tungsten- and titania-hydroxyapatite composites as well as titania-CNT composites as shown in **Figure 2**; note that no phase changes were detected after treatment (Figure S1, Supporting Information). Their evolution was broadly similar as described for titania, however differences were found in the size and yield of particles formed. There was only a small reduction (average ca. 5%) in surface area between PTX and PBM particles as measured by BET (Table S1, Supporting Information). Adsorption-desorption isotherms (Figure S2, Supporting Information) demonstrated a narrow and steep hysteresis loop at high relative pressures. Following PBM formation, the hysteresis loop shifted slightly to higher relative pressures indicating a coarsening of nanoporosity. Pore

size and volume approximation indicated a loss in pores 3 - 10 nm in size and a reduction in pores 10 - 25 nm in diameter upon PBM formation. Mercury porosimetry however did not reveal any changes in pore size distribution between 10-100 nm for titania or hydroxyapatite PBM (Figure S3, Supporting Information).

Wet PBM were at least four times stronger than the PTX from which they were formed in all samples measured, and in some instances the strength of the xerogels could not even be determined since they fragmented upon contact with water or during sample manipulation into the measuring position (Figure 2a and Table S1, Supporting Information). Tungsten PBM appeared to be an exception since it fragmented in water, but was 1.7 MPa in ethanol. Stability was assessed by dynamic light scattering (DLS) counts of water in which PBM were refluxed for an hour or after repeated cycles of drying and wetting (Figure S4, Supporting Information). No nanoparticle generation was observed by DLS and this was confirmed by ultracentrifuging the supernatant and examination using transmission electron microscopy (data not shown). Mechanical properties were also unaltered by this procedure (Figure 2a).

PBM formation was found to be dependent upon H· but not OH· radicals since ultrasound exposure of PTX in the presence of H· scavengers resulted in complete fragmentation similar to PFC samples (Figure 1b,c), whereas PBM assembly was unaffected by the presence of OH· scavengers (Figure S5, Supporting Information). H· scavenger efficiency was confirmed by KI oxidation dosimetry^[21] (SE_{KI}) which was greatly reduced from 64.0 ± 5.1 to 3.7 ± 0.9 pmol J⁻¹ with the addition of chloride ions, but only to 48 ± 3.5 pmol J⁻¹ when sucrose was added as an OH· scavenger.

Careful displacement of air from dry PTX by wicking water in and leaving a gas ‘escape route’, rather than full liquid immersion which trapped bubbles in the gel, eliminated surface

cavitation and subsequent PBM formation and identical results were obtained by placing the PTX under vacuum to expel the entrapped air prior to wetting. Therefore, localization of cavitation events at the xerogel surface and the generation of H· radicals seemed to be required for PBM formation. H· radicals are known to be extremely short-lived^[22] and if they are involved in the strengthening of these gels they would need to be generated at the particles' surface in order to modify it. In addition to water, isopropyl alcohol (IPA) and glacial acetic acid could be used to form PBM whereas toluene and DMSO were not suitable. A common feature of the effective solvents appeared to be their protic and polar nature.

Having established that a phosphate coating was essential for PBM formation, an optimum concentration of 5 wt% was observed to give the highest yield of TiO₂ PBM (Figure S6, Supporting Information). This amount corresponds to a theoretical phosphate coverage of ~20 % of the available surface. No evidence of crystalline sodium phosphate was detected through diffraction or electron microscopy in either PTX or PBM. After PBM formation with PTX containing 5% orthophosphate, the quantity of phosphate in the PBM reduced to 3 wt%, measured using inductively coupled plasma optical emission spectrometry (ICP-OES), suggesting some dissolution prior to bonding. The degree of protonation of orthophosphate did not seem important since PBM formation could be replicated with phosphoric acid and mono and di sodium acid phosphates. However, substitution of 5 wt% orthophosphate in this process with 5 wt% sodium pyro-, tri- and poly-phosphates, nitrate or sulphate salts did not result in the formation of visible PBM and at this scale, fragmentation behaviour appeared to be identical to PFC. In exploring possible reactions of trisodium phosphate with ultrasound in IPA, we found that there were changes in the hydration and protonation of this salt (Figure S7, Supporting Information), but no conversion to crystalline pyro- or poly-phosphate phases was detected.

We tested the hypothesis that localized heating thought to occur during cavitation^[23] could have melted the surface adsorbed phosphates into a glassy polyphosphate phase^[24] that fused the nanoparticles together. Titania PTXs made with either sodium or potassium phosphate were heated in a furnace to form Graham's or Kurrol salt glasses respectively on the surface of the nanoparticles.^[24] As little as 0.6% phosphate yielded sufficient glass to fuse the xerogel into a monolith that could withstand handling, but when these were added to water the particles disintegrated in all cases (Figure S8, Supporting Information).

PBM could be formed using either 20 or 42 kHz ultrasound; there was no difference in SE_{KI} at either frequency at 0.9 W cm⁻² power, (65.7 ± 8.0 vs. 64.0 ± 5.1 pmol J⁻¹ respectively) in good agreement with previous studies.^[21] Lowering the ultrasonic power below 0.9 W cm⁻² resulted in slower formation of PBM down to 0.2 W cm⁻², after which formation was prevented altogether, and increasing it to above 1.4 W cm⁻² caused fragmentation of PTX without assembly into PBM, likely because at this power the PBM was too weak to withstand these conditions. .

Adsorption of safranin O after 1h on NiO was very similar for nanoparticles and PBM (2.6 ± 1.7 vs. 2.9 ± 0.9 $\mu\text{g mg}^{-1}$), however methylene blue adsorption on TiO₂ PBM was higher than on nanoparticles (4.4 ± 0.7 vs. 0.8 ± 0.6 $\mu\text{g mg}^{-1}$). Ultrasonic cavitation is oxidizing and is known to convert FeO into Fe₂O₃^[25] and to oxidise titania,^[26] such a process may have increased the negative charge of the surface of TiO₂, whereas NiO is already highly negatively charged.^[27] No change in photocatalytic activity was observed for TiO₂ or NiO PBM compared with dispersions of native nanopowders (Figure 2 b,c). Repeated adsorption of methylene blue followed by UV catalysis of 18 μM MB in 1 hour for 20 cycles resulted in no change in catalytic activity of TiO₂ PBM. Phosphate glass coated xerogels (0.6 to 5 wt%) however had reduced photocatalytic rates of between 30 to 70 % (Figure S7, Supporting

Information), suggesting that the 3 wt% phosphate in PBM was not predominantly present as a glass.

The translation of nanoscale materials into the 3rd dimension is challenging^[28] and prevents the development of volume-efficient devices. Recently an electrodeposited cobalt phosphate (CoPi) catalyst was reported with the lowest water oxidation potential ever reported at pH 7.^[13, 14, 29] We were able to process this hydrated material (10.5 wt% weight loss from 110-400 °C) into conductive CoPi-CNT PBM composites some 200 μm in diameter (**Figure 3a,b**). Using a fixed area of fluorine doped tin oxide (FTO) coated glass electrode, current density with respect to water oxidation indicating oxygen evolution reaction (OER) for a conventional 2D electrodeposited electrocatalyst was compared with a 1 mm thick 3D electrode made from CoPi-CNT PBM in a nafion polymer. A large (15 X) increase in OER was only observed for CoPi-CNT PBM and not simple admixtures of the components or CoPi PBM without CNT (Figure 3c,d). These results indicate that the conductive CNT phase enhanced electron transfer from the semiconducting CoPi phase to the ITO electrode in PBM indicating electrically conductive and intimate contact between the phases. CoPi-CNT PBM electrodes achieved a 5 h oxygen evolution rate of 85.8 ± 5.2 compared to $36.2 \pm 4.8 \mu\text{mol O}_2 \text{ cm}^{-2}$ for conventional 2D electrodes (n=3) in cobalt ion free phosphate buffer (pH 7) and no change in performance was detected after 6.5 h operation (Figure S9, Video S1, Supporting Information). The inconsistency between electrochemical activity and oxygen evolution indicates that the rate limiting step may have been the oxygen–oxygen bond reaction to form oxygen molecules or the release of formed gas from the substrate.^[16, 30] Nonetheless, the applicability of this simple approach to improving performance of many 2D nanomaterial systems is self-evident. As observed in our prior experiments, the absence of a phosphate coating or the addition of H· scavengers prevented CoPi-CNT PBM formation and also subsequent electrical contact between CoPi and CNT (Figure 3c).

Survey and high resolution XPS of TiO₂ and CoPi-CNT did not reveal speciation differences between PTX and PBM (Figure S10, Supporting Information). Our data then indicate a very subtle change in surface chemistry had occurred during PBM formation. The increase in strength not being accompanied by an increase in density points to a change in the bond type between primary nanoparticles. The apparent involvement of H· radicals in this process is intriguing since very little is known about these extremely short lived ($\sim 10^{-6} - 10^{-7}$ s) species.^[22] We postulate that the conditions created during bubble cavitation either on or in the air-filled PTX form phosphate radicals, the product of the phosphate ion oxidation, having a half-life of about 300 ps at room temperature.^[31] These radicals could theoretically form phosphates and oxyphosphates at the surface of the PTX nanoparticles.^[32] Covalent bonding of these phosphate surfaces at collision points between xerogel fragments with the potential to bridge nanoparticles might reasonably be expected given reports of mechano-^[33] and ultrasonic^[34] induced reaction of a variety of metal phosphates and oxyphosphates. The low levels of phosphate present frustrated characterization, but treatment with phosphatase solution at pH 7.4 and 9 selecting pyrophosphatase and phosphatase activities respectively^[35] did not cause any fragmentation of PBM, neither did treatment in either 1N HCl or 1N NaOH at 100 °C for 6 h, known to degrade linear and cyclical polyphosphates, or calcining to 300 °C for 2 h followed by immersion in water. These data seem to reject the notion of phosphate glass fusion of nanoparticles being the cause of PBM and point towards considerable potential for using what we term ionic welding to manipulate nanoparticles into functional materials.

Although ultrasonic cavitation phenomena have been observed for decades and sonically generated radicals and cavitation are widely employed in chemical and particulate synthesis to good effect,^[1, 2, 36] there has been little progress in capitalizing on the reportedly huge localized temperatures and associated radical formation to build new materials from

particulate precursors. To the best of our knowledge this is the first time that the normally destructive forces of ultrasonic cavitation and associated radical formation have been applied to the microscale assembly of preformed nanoparticles whilst simultaneously retaining nanoscale functionality. The discovery of the interaction of surface adsorbed orthophosphate with cavitation events offers materials science a new tool for the creation of a multitude of new functional nanocomposites.

Experimental

Microparticle synthesis and self-assembly

Titanium Dioxide nanopowder (Aeroxide® P25 TiO₂, Ø ~ 20 nm) was supplied by Evonik Industries (Parsippany, NJ), Tungsten nanopowder (W, 99.95+%, Ø 40-60 nm) was supplied by US Research nanomaterials Inc. (Houston, TX), Nickel (II) oxide nanopowder (NiO, Ø < 50 nm), carbon nanopowder (C, Ø < 50 nm) and carbon nanotubes (CNT, multiwalled, Ø 6 - 9 nm) were supplied by Sigma Aldrich Canada (Oakville, ON). All other chemicals used were of reagent grade or better and were supplied by Sigma Aldrich Canada, unless stated otherwise. Nanocrystalline hydroxyapatite (Ca₁₀(PO₄)₆OH₂, Ø < 40 nm) was precipitated following the method of Jarcho *et al* [37]. Silver nanoparticles were synthesized by slowly adding 1 mL 100 mM aqueous silver nitrate solution to 100 mL of boiling 7 mM sodium citrate solution at pH 7. The reaction was then refluxed for 30 minutes. Cobalt phosphate catalyst (CoPi) was formed following the method of Kanan *et al.* [13]. Briefly, catalyst films were electrodeposited on fluorine-doped tin oxide (FTO) electrodes (Pilkington TEC7 Glass™) by controlled potential electrolysis of a 0.5 mM Co(NO₃)₂ aqueous solution in 100 mM potassium phosphate buffer at pH 7.0. Electrolysis was performed at 0.85 V (vs. Ag/AgCl) for several hours depending on the desired catalyst film thickness. After deposition, the electrodes were rinsed with deionized water and allowed to air-dry before carefully

removing and collecting the catalyst using a razor blade. Prior to mixing with CoPi particles, CNT were suspended in isopropyl alcohol (IPA) at a concentration of 1 mg mL⁻¹ and sonicated for 5 minutes to thoroughly disperse them. Immediately afterwards an aliquot of this suspension was mixed with CoPi to give a final CNT concentration of 0.3 wt%.

In order to create PTX, Na₃PO₄ or H₃PO₄ solutions (Fisher Scientific and Sigma Aldrich Canada respectively) were added to nanoparticulate powders in aqueous solution (0.025 – 3.33 mM g⁻¹). Assuming a P-O bond length of 150 pm [38] and a surface area for each surface of the PO₄ tetrahedron of 3 x 10⁻²⁰ m², the relative surface coverage of PO₄³⁺ ions to the nanoparticulate powders was calculated and concentrations adjusted accordingly to give between 0.5 – 100 % coverage. Following mixing, the pastes were dried at 100 °C to form a granular xerogel, which was then lightly crushed in a pestle and mortar to give the PTX starting material. PTX were then suspended in a range of solvents (water, isopropanol, acetic acid, toluene, DMSO) at a concentration of 0.5 – 10 wt / vol %. Typically water or IPA was used, having identified them as suitable, and treated with ultrasound using an unmodified benchtop ultrasonic bath (Branson UltraSonic Model 1510 MT, 42 kHz, 70 W) for times of 1-60 minutes. Microscale PBM were separated from unagglomerated nanoparticles by washing through a 53 µm sieve.

Supporting Information

Supporting Information is available online from Wiley InterScience or from the author

Acknowledgements

Mr R. Roy (McGill University) for assistance with ICP-OES measurements. Prof. R. Hill (McGill University) for helpful discussions. Prof. G. P. Demopoulos (McGill University) for the use of a solar simulator. Prof. J. A. Finch (McGill University) for the loan of a potentiostat. Pilkington Glass Ltd. for a generous donation of FTO glass. Supported by

NSERC Nano IP award (D.C.B.), NSERC Discovery Grant, NSERC Strategic Grant, Canada Foundation for Innovation and Canada Research Chair (J.E.B.)

Received: ((will be filled in by the editorial staff))

Revised: ((will be filled in by the editorial staff))

Published online: ((will be filled in by the editorial staff))

- [1] N. K. Bourne, *Shock Waves* **2002**, *11*, 447.
- [2] J. H. Bang, K. S. Suslick, *Adv. Mater.* **2010**, *22*, 1039; D. G. Shchukin, E. Skorb, V. Belova, H. Mohwald, *Adv. Mater.* **2011**, *23*, 1922.
- [3] S. Sharifi, S. Behzadi, S. Laurent, M. L. Forrest, P. Stroeve, M. Mahmoudi, *Chem. Soc. Rev.* **2012**, *41*, 2323; M. J. McCall, *Nat. Nanotechnol.* **2011**, *6*, 613; C. L. S. Wiseman, F. Zereini, *Sci. Total Environ.* **2009**, *407*, 2493.
- [4] T. Valdes-Solis, A. B. Fuertes, *Mater. Res. Bull.* **2006**, *41*, 2187.
- [5] G. W. Scherer, D. M. Smith, *J. Non-Cryst. Solids* **1995**, *189*, 197.
- [6] K. E. Parmenter, F. Milstein, *J. Non-Cryst. Solids* **1998**, *223*, 179.
- [7] N. Leventis, C. Sotiriou-Leventis, G. H. Zhang, A. M. M. Rawashdeh, *Nano Lett.* **2002**, *2*, 957.
- [8] Y. Q. Wang, X. H. Tang, L. X. Yin, W. P. Huang, Y. R. Hacohen, A. Gedanken, *Adv. Mater.* **2000**, *12*, 1183.
- [9] S. J. Doktycz, K. S. Suslick, *Science* **1990**, *247*, 1067; T. Prozorov, R. Prozorov, K. S. Suslick, *J. Am. Chem. Soc.* **2004**, *126*, 13890; D. Radziuk, D. Grigoriev, W. Zhang, D. Su, H. Mohwald, D. Shchukin, *J. Phys. Chem. C* **2010**, *114*, 1835.
- [10] P. Buffat, J. P. Borel, *Phys. Rev. A* **1976**, *13*, 2287.
- [11] S. Ramesh, Y. Koltypin, A. Gedanken, *J. Mater. Res.* **1997**, *12*, 3271.
- [12] N. Enomoto, S. Maruyama, Z. Nakagawa, *J. Mater. Res.* **1997**, *12*, 1410.
- [13] M. W. Kanan, D. G. Nocera, *Science* **2008**, *321*, 1072.
- [14] M. W. Kanan, Y. Surendranath, D. G. Nocera, *Chem. Soc. Rev.* **2009**, *38*, 109.
- [15] S. Cobo, J. Heidkamp, P. A. Jacques, J. Fize, V. Fourmond, L. Guetaz, B. Jousselme, V. Ivanova, H. Dau, S. Palacin, M. Fontecave, V. Artero, *Nat. Mater.* **2012**, *11*, 802.
- [16] Y. Surendranath, M. W. Kanan, D. G. Nocera, *J. Am. Chem. Soc.* **2010**, *132*, 16501.
- [17] A. G. Evans, M. E. Gulden, M. Rosenblatt, *Proc. R. Soc. London Ser. A-Math. Phys. Eng. Sci.* **1978**, *361*, 343; J. G. Chacon-Nava, F. H. Stott, S. D. de la Torre, A. Martinez-Villafane, *Mater. Lett.* **2002**, *55*, 269.
- [18] L. Duffours, T. Woignier, J. Phalippou, *J. Non-Cryst. Solids* **1995**, *186*, 321.
- [19] T. Terao, T. Nakayama, *Phys. Rev. E* **1998**, *58*, 3490.
- [20] E. C. D. Lima, F. Galembeck, *J. Colloid Interface Sci.* **1994**, *166*, 309.
- [21] S. Koda, T. Kimura, T. Kondo, H. Mitome, *Ultrason. Sonochem.* **2003**, *10*, 149.
- [22] R. Roots, S. Okada, *Radiat. Res.* **1975**, *64*, 306.
- [23] J. Rae, M. Ashokkumar, O. Eulaerts, C. von Sonntag, J. Reisse, F. Grieser, *Ultrason. Sonochem.* **2005**, *12*, 325.
- [24] I. S. Kulaev, V. M. Vagabov, T. V. Kulakovskaya, *The biochemistry of inorganic polyphosphates*, J. Wiley, Chichester, West Sussex; Hoboken, NJ : **2004**.
- [25] E. Kowalska, J. Mizera, *Przem. Chem.* **1969**, *48*, 210.
- [26] N. Sakai, R. Wang, A. Fujishima, T. Watanabe, K. Hashimoto, *Langmuir* **1998**, *14*, 5918.
- [27] N. Hernández, R. Moreno, A. J. Sánchez-Herencia, J. L. G. Fierro, *J. Phys. Chem. B* **2005**, *109*, 4470.
- [28] R. K. Joshi, J. J. Schneider, *Chem. Soc. Rev.* **2012**, *41*, 5285.
- [29] Y. Surendranath, M. Dinca, D. G. Nocera, *J. Am. Chem. Soc.* **2009**, *131*, 2615.

- [30] Y. Surendranath, Ph.D, Massachusetts Institute of Technology, **2011**; J. Jirkovsky, M. Makarova, P. Krtil, *Electrochim. Commun.* **2006**, *8*, 1417.
- [31] J. R. Huber, E. Hayon, *J. Phys. Chem.* **1968**, *72*, 3820.
- [32] Y. C. Tang, X. H. Huang, H. Q. Yu, L. H. Tang, *Int. J. Photoenergy* **2012**.
- [33] M. N. Kislitsyn, A. B. Yaroslavtsev, *Solid State Ionics* **2003**, *162*, 197.
- [34] Y. Y. Fan, Z. C. Hu, J. Yang, C. Zhang, L. Zhu, *Appl. Surf. Sci.* **2013**, *266*, 22.
- [35] Y. Xu, T. F. Cruz, K. P. Pritzker, *J. Rheumatol.* **1991**, *18*, 1606; A. Mizutani, R. J. Barnett, *Nature* **1965**, *206*, 1001.
- [36] C. E. Brennen, *Cavitation and bubble dynamics*, Oxford University Press, New York : **1995**; K. S. Suslick, G. J. Price, *Annu. Rev. Mater. Sci.* **1999**, *29*, 295.
- [37] M. Jarcho, C. H. Bolen, M. B. Thomas, J. Bobick, J. F. Kay, R. H. Doremus, *J. Mater. Sci.* **1976**, *11*, 2027.
- [38] B. Gamoke, D. Neff, J. Simons, *J. Phys. Chem. A* **2009**, *113*, 5677.

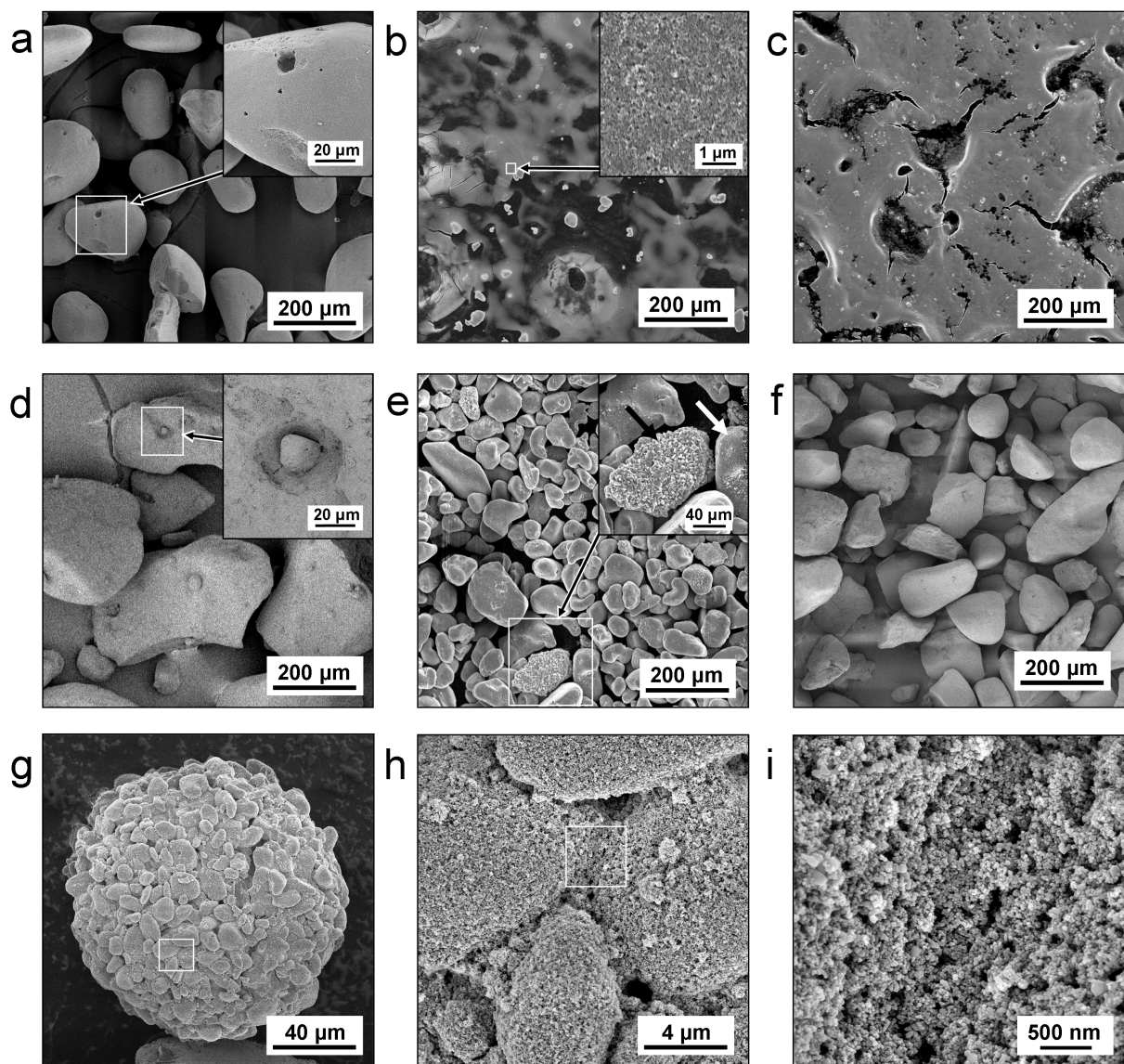


Figure 1: Scanning electron micrographs of TiO₂ PFC showing gradual disintegration after **a)** 5 mins **b)** 30 mins and **c)** 60 mins ultrasound treatment, and **(d-f)** TiO₂ PTX at the same timepoints. Inserts in a and d show surface details of the cavitation pits. Insert in e is a high

magnification SEM of a PBM intermediate. The black arrow points to a microparticle consisting of rounded agglomerates of phosphate bonded gel fragments and the white arrow indicates a homogeneous and presumably ‘mature’ PBM in which the individual particles have consolidated but rough surface texture is still evident. Closer inspection of the intermediate stage PBM revealed that the individual particles from which they were assembled were clearly discernible (**g**), inter-particle bridges were formed from nanoparticulate gel (**h**), however the nanostructure appeared homogeneous in both particles and bridges (**i**).

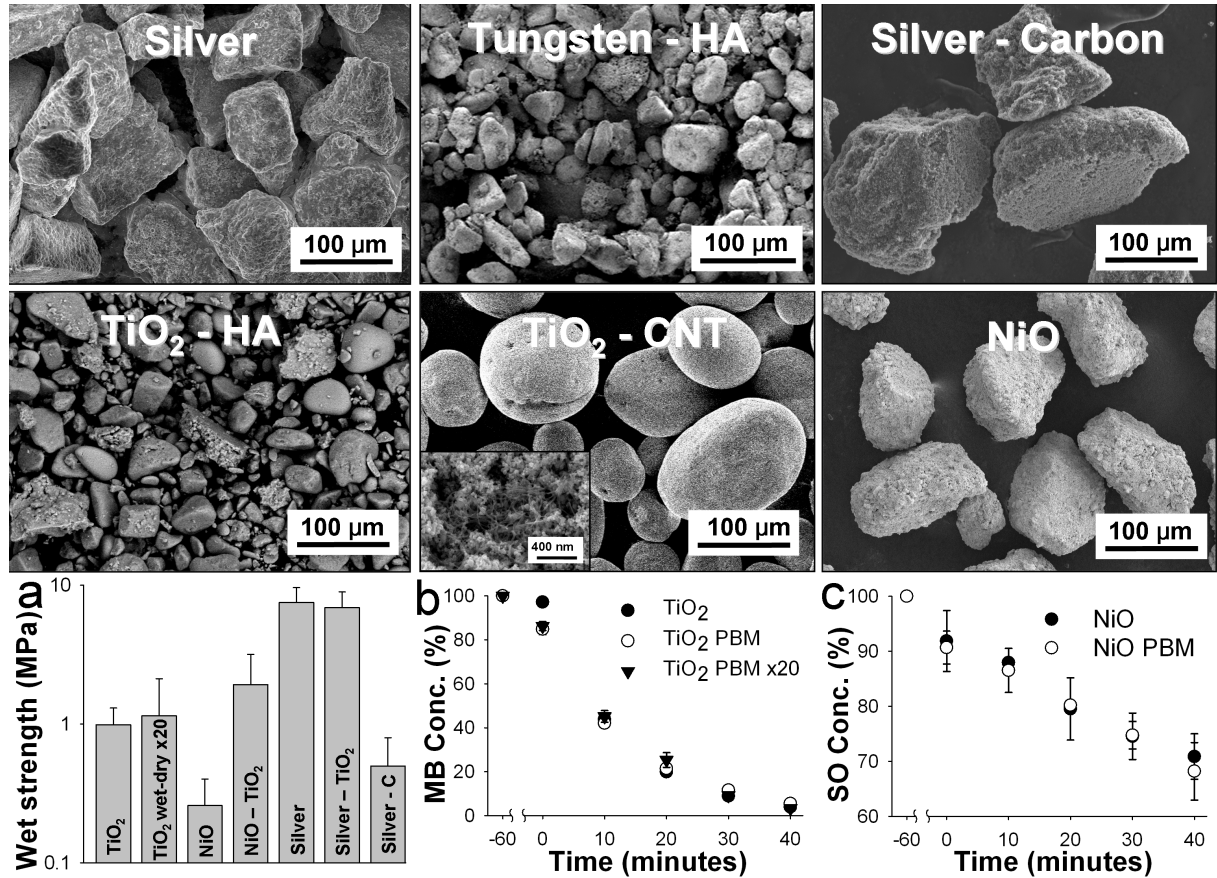
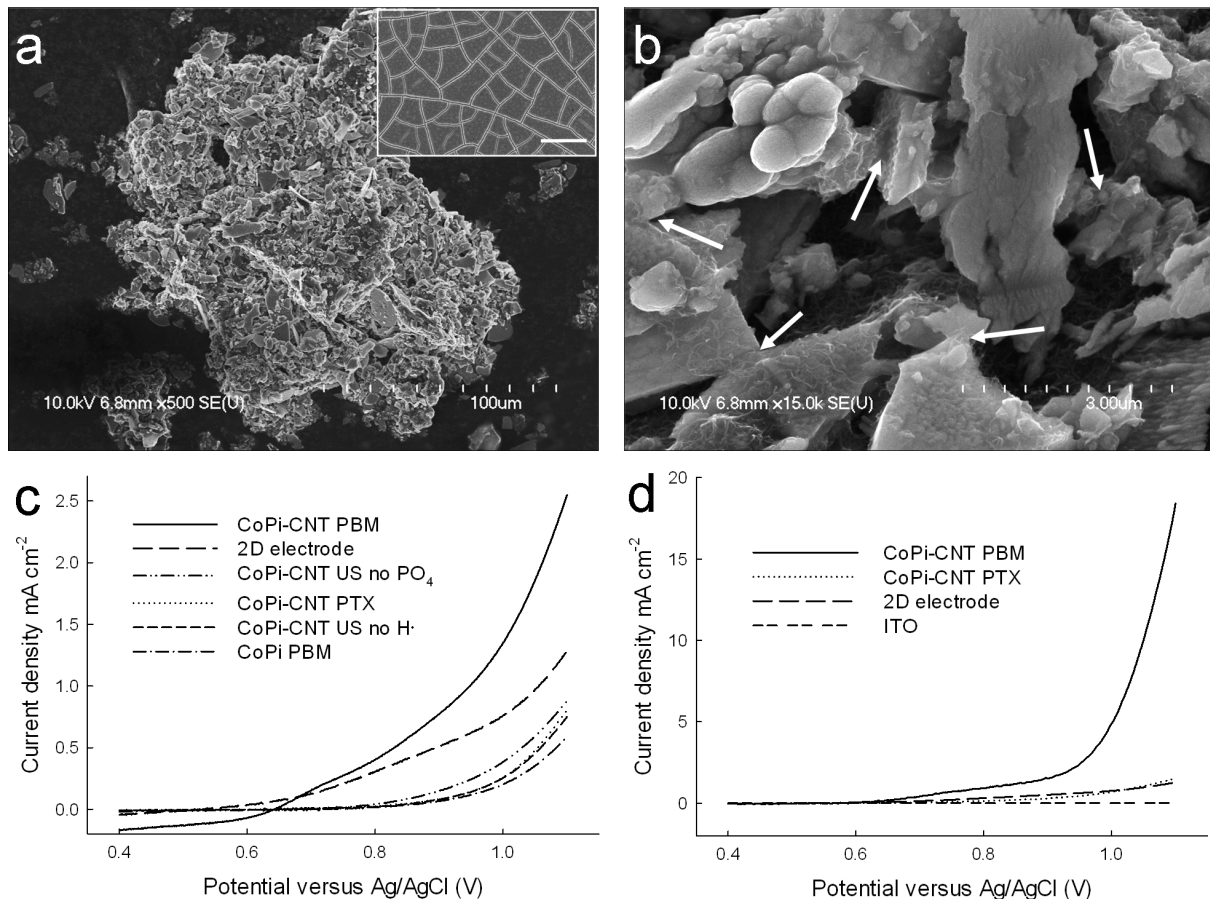


Figure 2: Scanning electron micrographs of washed PBM and composites (HA – hydroxyapatite, CNT – carbon nanotubes). **a)** Tensile strengths of PBM in water. TiO₂ wet-dry was repeatedly dried and rehydrated for 20 cycles and measured again. **b)** Photocatalytic activities as determined by the degradation of methylene blue (MB) under UV irradiation of: colloidal dispersion of TiO₂ nanopowder, TiO₂ PBM and TiO₂ PBM after 20 repeated photocatalytic activity tests (TiO₂ PBM X20) showing no loss in activity. **c)** Photocatalytic activity of NiO compared to NiO PBM under simulated solar irradiation as determined by the degradation of safranin O (SO).

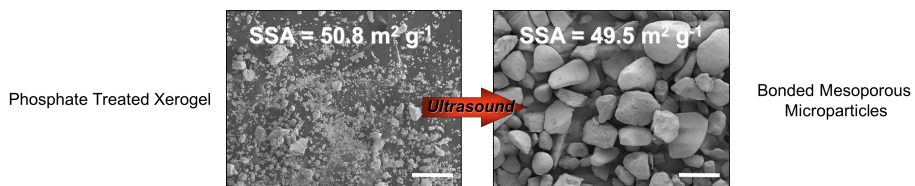


The table of contents entry

David C Bassett, Geraldine Merle, Bruce Lennox, Reza Rabiei, François Barthelat, Liam M Grover *and* Jake E Barralet

Ultrasonic phosphate bonding of nanoparticles.

Low intensity ultrasound-induced radicals interact with surface adsorbed orthophosphate to bond nanoparticles with high mechanical strength and surface area. Dissimilar materials could be bonded to form robust metallic, ceramic and organic composite microparticles. 3D nanostructures of a hydrated and amorphous electrocatalyst with carbon nanotubes were also constructed which exceeded the resistance-limited efficiency of 2D electrodes.



ToC figure ((55 mm broad, 50 mm high, or 110 mm broad, 20 mm high))

Supporting Information

Experimental

Parameters of PBM formation

To investigate the effect of alternative anions on PBM formation, orthophosphate was substituted with tetra- and di-sodium pyrophosphate, sodium tri- and poly-phosphate, sodium nitrate and sodium sulphate for the formation of TiO₂ xerogels at a concentration sufficient to give a 20 % anion surface coverage prior to drying and ultrasound exposure.

The effect of power on PBM formation was investigated using an ultrasonic horn equipped with a power modulation control and 5/32" microtip (Omni Sonic Ruptor 250, 20 kHz, 0-250 Watts, OMNI International Inc. Marietta, GA). The ultrasonic power of this instrument and the Branson ultrasonic bath were calculated by measuring the temperature rise per second (dT/dt) of 20 cm³ water due to sonication over time and using the following equation:

$$\text{Power (W)} = \frac{dT}{dt} CpM \quad (1)$$

where Cp is the heat capacity of water (4.2 J g⁻¹) and M is the mass of water.

To test the effect of free radical scavengers on the ultrasound driven self assembly process the following chemicals were added: H· radical scavengers: 2.5 vol % H₂O₂, 10 mM NO₃⁻, SO₄²⁻, and Cl⁻ ions presented as sodium salts; OH· radical scavengers: 2.5 vol % methanol, 2.5 vol % acetic acid, 10 mM sucrose (C₁₂H₂₂O₁₁). KI oxidation dosimetry, as described previously [1], was used to quantify the sonochemical efficiency with and without radical scavengers (10 mM Cl⁻ and sucrose). Briefly the ultrasonic dependant formation of I₃⁻ from 100 mM KI solution was measured by optical absorption at 355 nm ($\epsilon = 2.6 \times 10^4$ dm³ mol⁻¹ cm⁻¹) and dividing this amount by the ultrasonic power (equation 1) multiplied by the duration of ultrasound exposure, to give the sonochemical efficiency (SE_{KI}) with units of mol J⁻¹.

To test the effect of wetting, TiO₂ PTX particles were hydrated slowly by sprinkling on moist filter paper to allow hydration by “wicking” prior to immersion in water. Finally TiO₂ PTX particles were evacuated in a Büchner flask to a pressure of ~ 17 kPa prior to introducing water through an attached valve. These pre-hydrated samples were then suspended in water and exposed to ultrasound.

TiO₂ PTX was also made with NaH₂PO₄ and KH₂PO₄ at concentrations of 0.625 – 5 wt % PO₄ and heated to 750 °C for 2 hours and 300 °C for 1 hour respectively. Samples were then crushed in a pestle and mortar, sieved in the range 53 – 125 µM. Sieved particles were then evaluated for photocatalytic activity as described below, and suspended in water and observed for particle fragmentation.

Characterization

SEM analysis was performed on Au-Pd coated samples using a Hitachi S-4700 FEG-SEM operating at an accelerating voltage of 2-10 kV (Hitachi, Tokyo, Japan). X-ray diffraction analysis was performed with Cu K α X-rays with a Bruker X-ray diffractometer (Model D8 DISCOVER, Bruker AXS, Inc. Madison, WI) across a 2 θ range of 5-50°. The diffraction spectra were processed using DIFFRACplus Eva (Version 7) software with reference to Powder Diffraction File database (PDF 4+ 2008) of the International Centre for Diffraction Data (Newton Square, PA). Specific surface area measurements were made using the Brunauer–Emmett–Teller (BET) method (TriStar 3000, Micromeritics, Norcross, GA) using nitrogen as the adsorbate. Pore volume was calculated from adsorption-desorption data using the Barrett-Joyner-Halenda (BJH) model. Samples were degassed under vacuum for 12 hours at 100 °C prior to analysis. To determine phosphorous concentrations in TiO₂ PTX and PBM, 0.1 g samples were leached for 12 hours at 60 °C in 20 mL aqua regia (3:1 HCl : HNO₃). The volume was then increased to 50 mL and samples were analysed for phosphorous at an optical

emission of 178.2 nm and compared to samples of known concentration using a Thermo Scientific iCAP 6500 ICP spectrometer (Fisher Scientific Ltd, Nepean, ON). Thermogravimetric analysis was performed using a TA Instruments Q600 DSC-TGA (TA Instruments, New Castle, DE) at a heating rate of 10 C min^{-1} to a temperature of $1200\text{ }^{\circ}\text{C}$ in an air flow. The micro-porosity of TiO_2 and HA PTX and PBM were analysed using a mercury porosimeter (AutoPore IV 9500, Micromeritics, Norcross, GA). X-ray photoelectron spectroscopy (XPS) was performed using a Thermo Scientific K-Alpha XPS (Fisher Scientific Ltd, Nepean, ON) fitted with a monochromatic Al $\text{K}\alpha$ X-ray source (1486.6 eV) with a spot size of 400 μm . 50 binding energy scans were taken of each element of interest using a pass energy of 50 eV, a dwell time of 50 ms and a step size of 0.1 eV. Instrument calibration was checked using Ag and Au standard samples and data was processed using Thermo Avantage software, taking a Shirley background approximation.

Mechanical Testing

Mechanical testing was performed following the methodology described by Dexter and Kroesberge [2] to determine the tensile strength of aggregates from compressive experiments. The tests were performed using a custom made loading stage composed of glass slides glued together at an offset to provide a platform 2 mm wide and 1 mm deep. The loading stage and sample were placed under an optical microscope (BX-51M, Olympus, Markham, Canada) equipped with a CCD camera (RETIGA 2000R, Qimaging, Surrey, Canada). A 5 lb load cell (Model 11-AT Subminiature Tension/Compression Load Cell, Honeywell, Columbus, OH) was mounted on a manual micromanipulator, and a square piece of glass 2 x 2 x 1 mm was attached to the load cell. Samples were loaded by manually moving the micromanipulator in the plane of the loading stage and recording the load at failure. Determination of statistical significance between mean strengths of wet PTX and PBM was determined using a student's

t-test (Microsoft Excel) when possible, since some PTX were so weak that samples broke while being manipulated in the testing stage.

TiO₂ PBM mechanical stability was assessed by measuring particle disintegration by dynamic light scattering (DLS - ZetaSizer Nano ZS, Malvern Instruments, MA, USA). The live count rate of scattered light from the supernatant of suspended particles was recorded following 10 minutes settling time, following 1 hour reflux in boiling water and then 10 minutes settling, and following 20 cycles of drying at 100 °C and rehydration and then final suspension and settling for 10 minutes. These values were compared to background count rates and those obtained for untreated TiO₂ nanoparticles and the supernatant of suspended TiO₂ nanoparticles following ultracentrifugation at 36,000 rpm for 30 minutes at 4 °C (Optima L-90 K ultracentrifuge fitted with an SW 41 rotor, Beckman Coulter Inc. Mississauga, ON). Dried and rehydrated samples were also mechanically tested again for a change in tensile strength. Additionally fragmentation of TiO₂ PBM was monitored following incubation 5 mg mL⁻¹ in 1 mg mL⁻¹ bovine ALP enzyme (Sigma-Aldrich, Canada) in TRIS Buffer at pH 9 and 1% DNase enzyme (Invitrogen, Carlsbad, CA) in TRIS buffer at pH 7.4 for 3 days at 37 °C. PBM stability was also tested following boiling for 6 hours in 1N HCl or 1N NaOH and by calcining at 300 °C for 2 h followed by immersion in water.

Catalytic activity evaluation

TiO₂ photocatalytic activity was determined by measuring the degradation of methylene blue (MB, C₁₆H₁₈N₃S, Fisher Scientific) in aqueous solution. 20 mg TiO₂ catalyst powder was suspended in 100 mL 18 µM MB under stirring in a light shielded enclosure maintained at 30 ± 2 °C by water cooling. UV illumination was provided by a 100 W long-wavelength (365 nm) high intensity UV spot lamp (Blak-Ray, Ted Pella, Redding, CA.) suspended at 15 cm

above the surface of the reaction medium, which provided a light intensity of approximately 15 mW cm⁻².

NiO photocatalytic activity was determined by measuring the degradation of safranin O (SO, C₂₀H₁₉N₄Cl, Sigma Aldrich) in aqueous solution. 20 mg NiO catalyst powder was suspended in 100 mL 18 μM SO under stirring. Uniform light approximating the AM 1.5 Global reference spectrum was provided by a small area solar simulator (PV measurements Inc., Model SASS) fitted with a tungsten lamp giving a light intensity of 100 mW cm⁻². Catalyst suspensions were magnetically stirred for 1 hour in complete darkness to establish adsorption-desorption equilibrium prior to light exposure. 1 mL aliquots were taken at various time-points and immediately centrifuged prior to adsorption measurements at 665 and 518 nm to determine MB and SO concentrations respectively using a UV-Vis-NIR spectrophotometer (Cary 5000, Varian, Palo Alto, CA).

The electrocatalytic activity of Co based materials was evaluated using a Parstat 2263 potentiostat (Princeton Applied Research, Oak Ridge, TN) fitted with a Ag/AgCl reference electrode and a Pt-wire counter electrode. All electrochemical measurements were performed at atmospheric pressure and ambient temperature. Polarization curves were recorded using a standard three electrode system in 100 mM potassium phosphate buffer, pH 7.0 and recorded after 10 cycles at a scan rate of 10 mV s⁻¹. 2D electrodes were prepared by casting an aqueous suspension of catalysts onto an FTO electrode of 1 cm² (loading ~ 1 mg cm⁻²). 3D electrodes were formed by gluing a 1.25 mm thick polypropylene mask with a 2.5 mm diameter hole with epoxy, either to the electrodeposited or the bare FTO electrode. The hole in the mask of the bare FTO electrode was filled with 250 μg of catalyst and 8 μL of 5% Nafion® perfluorinated resin solution (Sigma Aldrich) were dispersed in 50 μL of 3:1 v/v water/ethanol mixed solvent to give a final loading of ~ 5 mg cm⁻².

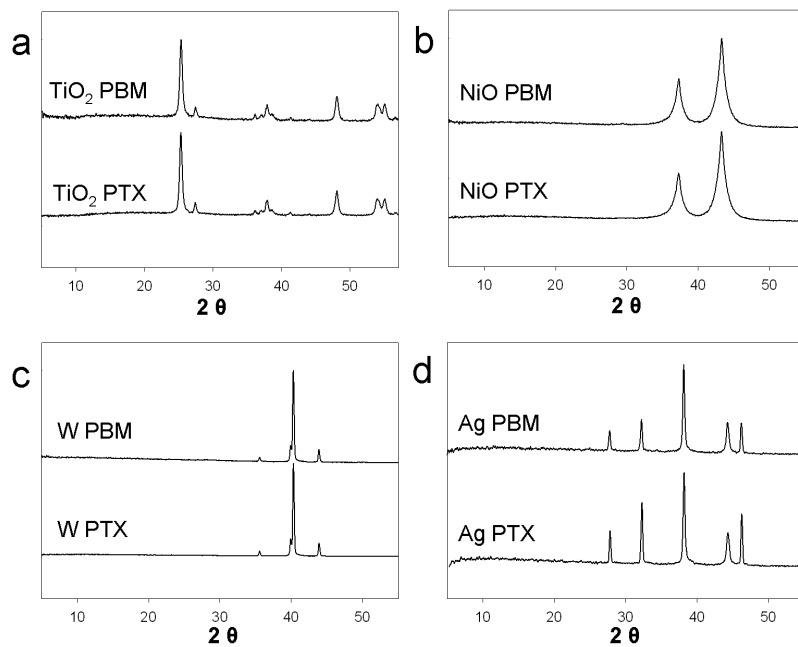


Figure S1: No phase changes were detected between as made PTX and following 1h ultrasound exposure for **a)**: Titanium dioxide, **b)**: Nickel oxide, **c)**: Tungsten or **e)**: Silver PBM.

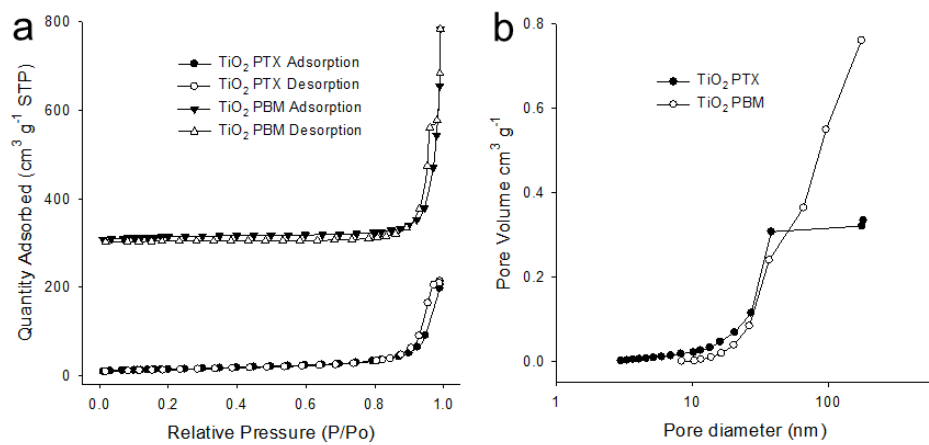


Figure S2: **a)** Comparison of nitrogen adsorption-desorption isotherms for TiO₂ PTX and PBM. TiO₂ PBM has been offset vertically by 300 $\text{cm}^3 \text{g}^{-1}$. **b)** Cumulative adsorption pore volume distributions showing a slight change in mesoporosity and a growth in pores between 50 - 200 nm.

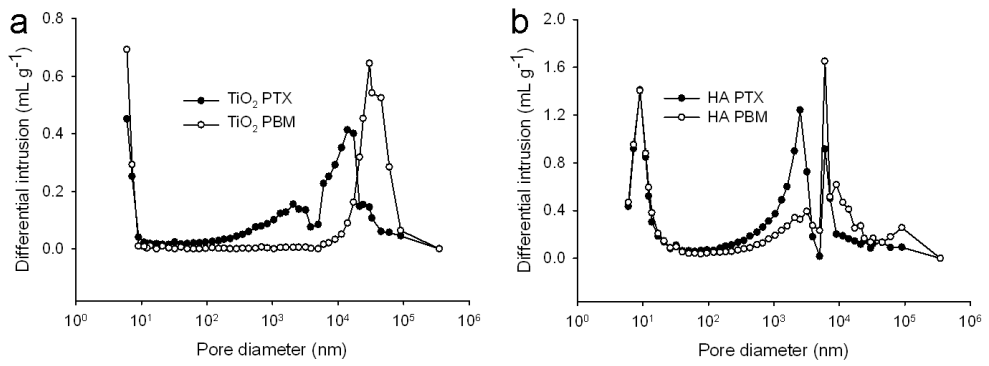


Figure S3: No change in mesoporosity (<50 nm) of **a**): TiO_2 and **b**): HA PBM during phosphate bonding of PTX as shown using mercury porosimetry, changes at the microscale indicate changes in gel granule size.

Table S1: Specific surface area and wet tensile strengths of PTX and PBM materials and composites. N/M not measurable: sample was too weak for measurement.

Material	SSA [m ² g ⁻¹]	Wet tensile strength [MPa]
TiO ₂ np	52.4 ± 0.1	-
TiO ₂ PTX	50.8 +/- 0.03	0.13 +/- 0.09
TiO ₂ PBM	49.5 +/- 0.32	0.99 +/- 0.31
W np	2.2 +/- 0.01	-
W PTX	2.0 +/- 0.03	N/M
W PBM	0.8 +/- 0.02 [a]	1.74 +/- 0.83
NiO np	152.1 +/- 0.8	-
NiO PTX	141.3 +/- 0.7	0.06 +/- 0.04
NiO PBM	139.3 +/- 0.8	0.26 +/- 0.14
TiO ₂ -NiO PTX	92.7 +/- 0.3	0.54 +/- 0.32
TiO ₂ -NiO PBM	90.3 +/- 0.4	1.92 +/- 1.24
Ag np	11.7 +/- 0.2	-
Ag PTX	11.9 ± 0.1	1.20 +/- 1.19
Ag PBM	10.0 ± 0.1	7.47 +/- 2.11
Ag-C PTX	367.6 ± 5.3	N/M
Ag-C PBM	365.0 ± 5.3	0.50 +/- 0.29
Ag-TiO ₂ PTX	36.2 ± 0.4	0.22 +/- 0.23
Ag-TiO ₂ PBM	34.0 ± 0.2	6.87 +/- 2.05

[a] SSA was low for this sample since it was found that the starting nanopowder possessed a much wider particle size distribution (up to 4 μm) than the manufacturer's specifications suggested, our processing technique appeared to preferentially select the larger particles as determined by scanning electron microscopy..

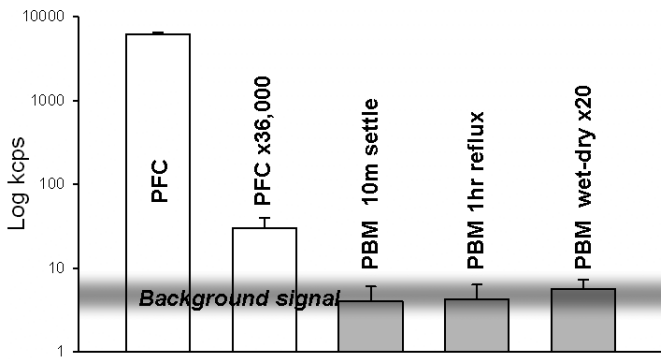


Figure S4: Stability of TiO₂ PBM compared with PFC as determined by the count rate (kcps) obtained from dynamic light scattering. A suspension of PFC TiO₂ at a concentration of 100 mg L⁻¹ after 10 minutes settling had considerable turbidity, and even after centrifuging at 36,000 rpm for 30 minutes appreciable turbidity remained in the supernatant (White bars). In contrast no turbidity was measurable for 100 mg TiO₂ PBM that had been washed through a 53 µm sieve, suspended in 100 mL water and allowed to settle under gravity for 10 minutes (10m settle), this remained the case following 1 hour reflux of the particles in water (1hr reflux) and repeatedly drying and rehydrating for 20 cycles (wet-dry x20), indicating the PBM did not fragment into constituent nanoparticles. Ultracentrifugation (36,000 rpm, 10 minutes) of the liquid in which the samples were aged, followed by examination of the lower portion of supernatant (20 x 10 µL drops on formvar coated nickel grid) using a transmission electron microscope did not reveal any evidence of primary nanoparticles, (data not shown). Background signal was determined by measuring the count rate of 1 mL sample of ultrapure water that had been filtered using a 0.22 µm syringe filter at the same laser height and attenuation settings used to measure the experimental samples.

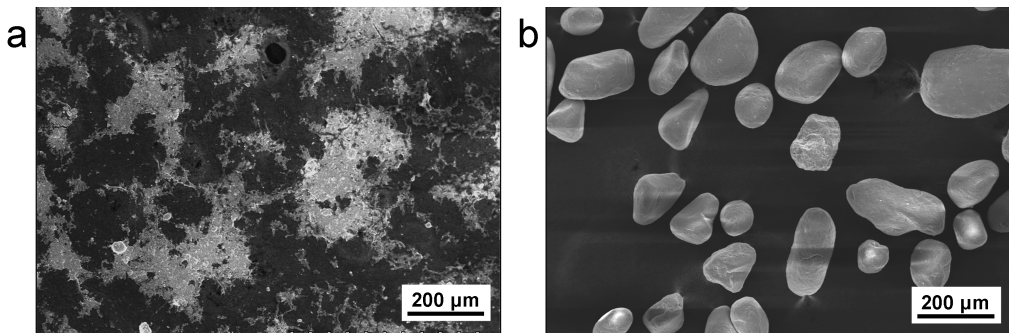


Figure S5: Exposure of PTX in the presence of a $\text{H}\cdot$ scavenger (chloride ions) resulted in complete fragmentation similar to PFC samples (**a**), whereas PBM assembly was unaffected in the presence of an $\text{OH}\cdot$ scavenger (sucrose) (**b**).

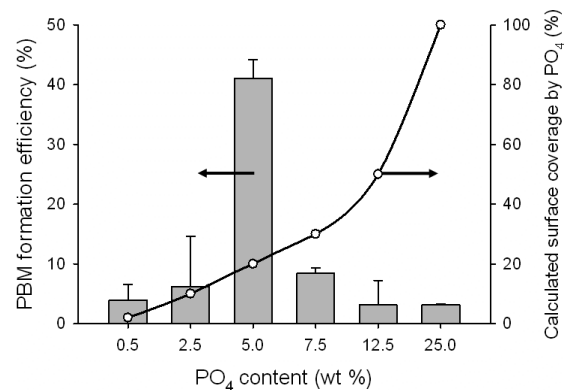


Figure S6: Efficiency of TiO_2 PBM formation as determined by the fraction of particles formed $> 53\mu\text{m}$ following 1 hour ultrasound exposure as a function of PO_4 content in the original PTX at a PTX solid fraction of 1 wt / vol %.

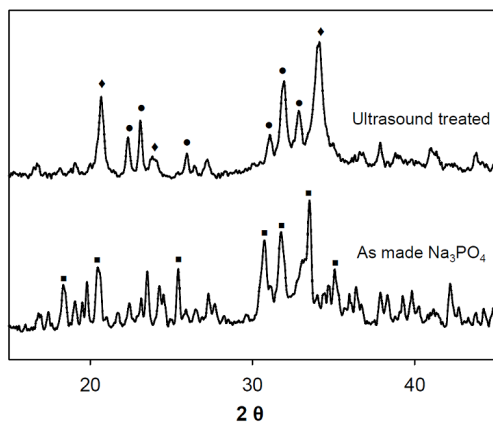


Figure S7: Ultrasound exposure of $\text{Na}_3\text{PO}_4 \cdot 8\text{H}_2\text{O}$ (■: PDF 00-037-0334) in IPA for 1 hour resulted in partial conversion to Na_2HPO_4 (●: PDF 01-076-2287) and dehydration of the Na_3PO_4 phase (◆: 00-031-1323).

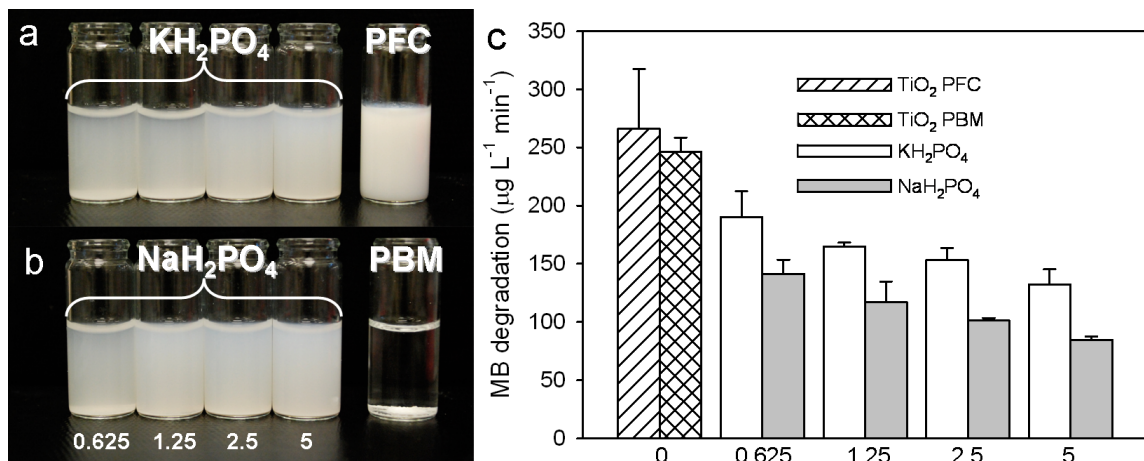


Figure S8: Visual appearance of TiO_2 PTX containing indicated amount (wt %) of Kurrol (a) or Graham's salt (b) phosphate glasses after having been sieved to a particle size range of 53 – 100 μm and then suspended in water at a concentration of 4 g L⁻¹ and settled for 10 minutes. Considerable turbidity was apparent in all samples, comparable to PFC nanoparticles, however complete settling occurred for PBM within 3 minutes. **c**): Photocatalytic activity of TiO_2 expressed as the rate of degradation of methylene blue (MB) was reduced in PTX treated with indicated amounts (wt%) of Kurrol or Graham's salt compared with TiO_2 PFC and TiO_2 PBM.

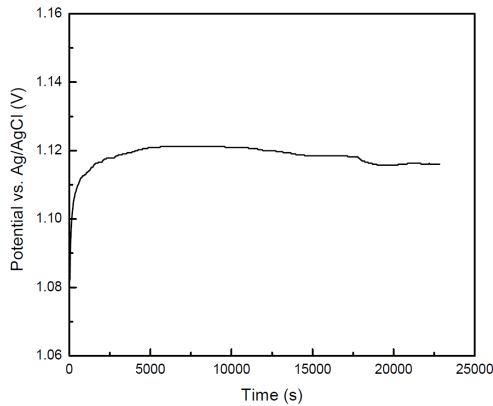


Figure S9: Chronopotentiometric curve obtained for the 3D electrode constructed using CoPi-CNT PBM in 0.1M potassium phosphate buffer (pH 7.0) and constant current density 16 mA cm⁻². Potential did not increase over a time of 6.5 hours indicating excellent stability of the electrode.

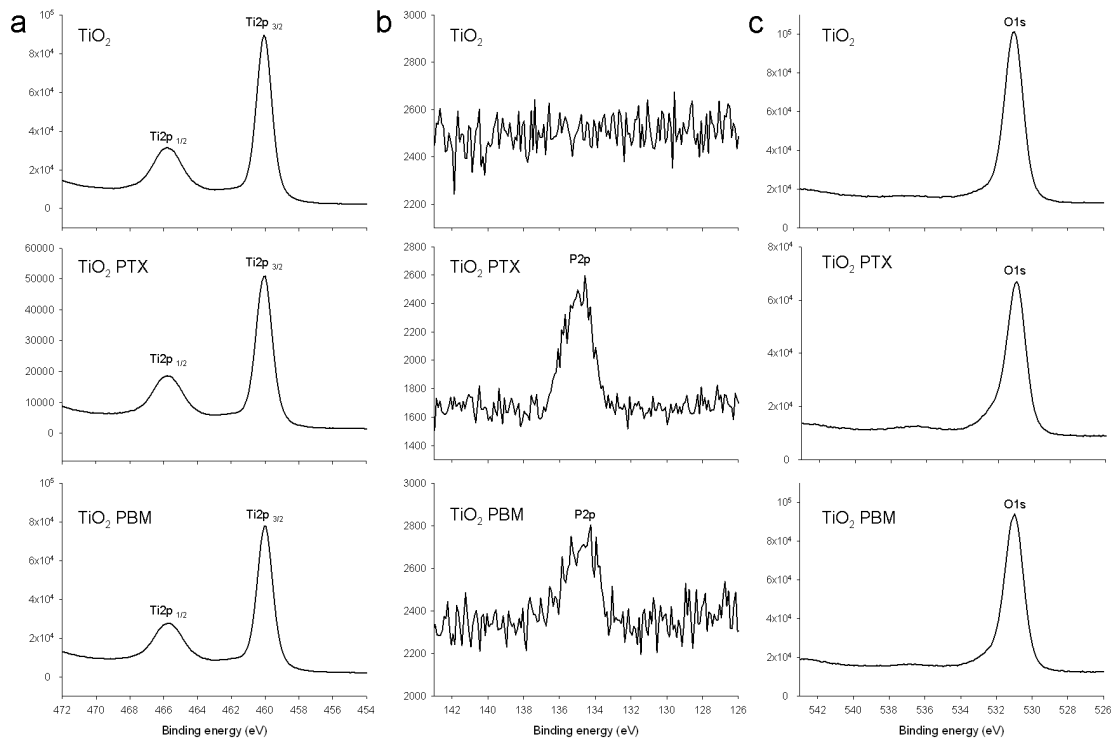


Figure S10: High resolution XPS spectra of TiO₂ (top row), TiO₂ PTX (middle row) and TiO₂ PBM (bottom row). **a)** Ti2p peaks. **b)** P2p peaks. **c)** O1s peaks. FWHM values did not vary for Ti2p_{3/2} and O1s and were 1.2 and 1.6 respectively for all samples which compare well with previously reported values [3].

References

- [1] S. Koda, T. Kimura, T. Kondo, H. Mitome, *Ultrason. Sonochem.* **2003**, *10*, 149.
- [2] A. R. Dexter, B. Kroesbergen, *J. Agr. Eng. Res.* **1985**, *31*, 139.
- [3] U. Diebold, T. E. Madey, *Surf. Sci. Spec.* **1996**, *4*, 227; B. Erdem, R. A. Hunsicker, G. W. Simmons, E. D. Sudol, V. L. Dimonie, M. S. El-Aasser, *Langmuir* **2001**, *17*, 2664.